UNIVERSITY *of* York

This is a repository copy of *Influence of Working Fluid on the Mean Flow Vortex Structure in Industrial Flow Pipelines of Arbitrary Bend Angle via RANS Simulation*.

White Rose Research Online URL for this paper:
https://eprints.whiterose.ac.uk/222209/

Version: Published Version

Book Section:

Church-Forbes, Keagan, Koshuriyan, Zamir and Abuhatira, Ahmed (2025) Influence of Working Fluid on the Mean Flow Vortex Structure in Industrial Flow Pipelines of Arbitrary Bend Angle via RANS Simulation. In: Baccouch, Mahboub, (ed.) Computational Fluid Dynamics - Analysis, Simulations, and Applications. IntechOpen , pp. 1-18.

https://doi.org/10.5772/intechopen.1008357

White Rose
university consortium
Universities of Leeds, Sheffield & York

eprints@whiterose.ac.uk
https://eprints.whiterose.ac.uk/

Chapter

Influence of Working Fluid on the Mean Flow Vortex Structure in Industrial Flow Pipelines of Arbitrary Bend Angle via RANS Simulation

Keagan Church-Forbes, Mohammad Zamir A. Koshuriyan and Ahmed A. Abuhatira

Abstract

Numerical simulations of flow through industrial pipelines is important for design purposes in commercial and domestic transport of oil and gas. In this paper we use steady Computational Fluid Dynamics (CFD) to investigate the effect of different working fluids and streamwise bend angle on the spatial distribution, wall shear stress and turbulence kinetic energy of the fully-developed Dean vortex. Using Ansys Fluent, steady Reynolds-Averaged Navier Stokes (RANS) simulations are performed in a parametric study for various gas flows (air, methane and carbon dioxide) and pipe elbow bend angles ($90°, 60°, 45°, 30°, 0°$). Our results show the flow properties (velocity streamlines, turbulence kinetic energy and induced wall shear stress) of the Dean vortex for inflow velocities ranging from 5 to 15 m/s at Dean numbers of $O(10^4)$ corresponding to working fluids having the same inflow mass flux. Reducing the pipe bend angle was found to minimize the wall shear stress and subsequent vortex magnitude for all gas flows types. We discuss these results quantitatively in terms of turbulent kinetic energy/the degree of secondary flow comparing to experimental literature. Reference to pipeline longevity is made.

Keywords: steady CFD, ANSYS fluent, secondary flow, dean vortices, wall shear stress

1. Introduction

Industrial flow pipelines will carry different fluids depending on their usage. For example, air is used in domestic heating, ventilation, and air conditioning (HVAC) systems; carbon dioxide (CO_2) is used in carbon capture, and storage applications, and methane in gas pipelines used to heat homes and buildings across the globe. It is often important to understand how these common gas flows behave when it comes to the design of pipelines used to transport them from one location to another and how the

different flow patterns within the fluids can affect both the structural integrity and overall life cycle of pipelines.

CO_2 is becoming of greater importance as we continue on the road to net zero where it is planned to be pumped underground in depleted wells across the North Sea for example. This will involve the transportation of CO_2 in pipelines with possibly multiple 90° bends when a change of flow direction is required. In such case, maintenance of pipeline systems requires understanding of the flow patterns along the pipe and particularly at the pipe elbow where the shear stress is largest. Other natural gases such as methane is an example of a natural gas that is used in household flows for cooking and heating. It is obviously crucial to understand how this gas behaves within bends in pipelines as it travels on its way to its destination. In this paper we assess the effect of pipe working fluid and bend angle on the mean flow vortex structure at the location of maximum flow shear stress (i.e. at the elbow along the inner pipe curve referred to as the *intrados* location). We accomplish this using Computational Fluid Dynamics (CFD) via steady Reynolds averaged Navier Stokes (RANS) simulations for pipe flow that is fully developed at inlet to the pipe elbow.

Pipe elbows are not only required for a change of flow direction in pipelines, they are also used to overcome man-made or geological obstacles along the pathway of the piping system. The pipe turning angle and radius of curvature are the two parameters that define the elbow. Although there may be some variety in their selection, the most common elbow joints being 45° and 90° but some can be greater or less than this depending on the requirements of the system or route for transportation of hydrocarbons, water, or other chemicals in a pipeline.

The impacts and effects of elbow joints are of great interest to researchers and have been explored both experimentally [1] and numerically in many different studies; see for example, refs. [2–11]. Sudo et al. [1] reported the secondary flow found immediately after the elbow location which was induced by the centrifugal force due to the elbow geometry and the primary flow was forced towards the outer wall. The experimental results produced by Sudo et al. have been replicated and validated by many authors, each with a slightly different aim. For example, similar secondary flow fluid mechanics were found in the numerical simulations published by Ganesh et al. [11]. The secondary flow results in swirling eddies close to the inner wall at the elbow outlet due to recirculation of flow [2, 7, 8, 11–13]. These eddies, known as *Dean vortices*, are counter rotating motions induced by pipe wall curvature and their numerical simulation is our focus here. That is, we use a commercial CFD code to parametrically investigate the wall shear stress and turbulence kinetic energy contours in the elbow region where the vortex motion persists. The main parameters in our simulations are the working gas fluid the pipe flow carries and the pipe bend angle. For self-consistency in the numerical analysis we consider fixed mass flow rate (equal to the baseline case of air in a 90° bend used by Church-Forbes et al. [16] who validated the experiments of Sudo et al. [1]) such that the flow coefficient of the pipe depends only on the specific gravity (and therefore the working gas flow under consideration) when the pressure drop is fixed. Note that the latter (pipe pressure drop) is set in CFD pre-processing as an input to the flow solver and is kept at the Church-Forbes et al./ Sudo et al. value.

2. CFD simulation of dean vortices in industrial pipelines

Dean vortices, visible near the inner (left hand side) wall location on the 90° location, are physically caused by the existence of a centrifugal force at the curved

inner elbow which creates a secondary flow in the pipe due to the primary (streamwise) flow being forced towards the outside wall [12]. They are described as a pair of counter-rotating vortices [14] located in the flow and can be seen to move further towards the middle of the pipe with less degree of swirl at reducing angle locations. Studies by Dutta et al. [2], Zhang et al. [13], Hufnagel et al. [8], and Röhrig et al. [5] also observed this swirling eddy flow at the inner wall at the 90° location in the elbow. To give an idea of the spatial morphology of these vortices, the streamlines produced by Dutta et al. [2] at 90° azimuthal location and at Reynolds number of 1×10^5 are shown in **Figure 1a**. The spatial distribution and maximum intensity of the Dean vortices found by Dutta et al. [2] were in good agreement with the CFD study by Wang et al. [12].

Turning our attention to the latter, Wang et al. [12] investigated the effects of pipe flow Reynolds number on the flow separation and secondary flow experienced in a 90° elbow with large curvature ratio (typically, $R_c/D > 0.5$) at various angles in the elbow from $(30° - 90°)$ using air as the fluid (see Dean number (De) definition below). Wang [12] found that the degree of boundary layer separation at the inner wall decreased with increasing Reynolds number (and as a consequence, increasing Dean number (De) at fixed curvature ratio) such that the Dean vortices displayed a higher degree of swirling due to turbulence increasing in the flow. Here, $De = Re \sqrt{D/2R_c}$, represents the ratio of viscous to centrifugal force acting in a curved pipe of Reynolds number, $Re = \rho U D/\mu$ based on pipe diameter, D, inflow pipe velocity U, where μ is the working fluid viscosity and R_c the radius of curvature of the inner pipe wall.

Kim et al. [3] attempted to replicate the results published by Sudo et al. [1] (which is used herein to establish a baseline test case) using Open Foam CFD software in order to further understand the secondary flow experienced at the elbow outlet. They found the swirl intensity of the eddies at the inner wall to be a strong function of the radius of curvature of the elbow and a weak function of Reynolds number. They also performed a comparative assessment to find the optimum k-ε turbulence model to use and found an RNG model provided sufficiently accurate results in comparison to
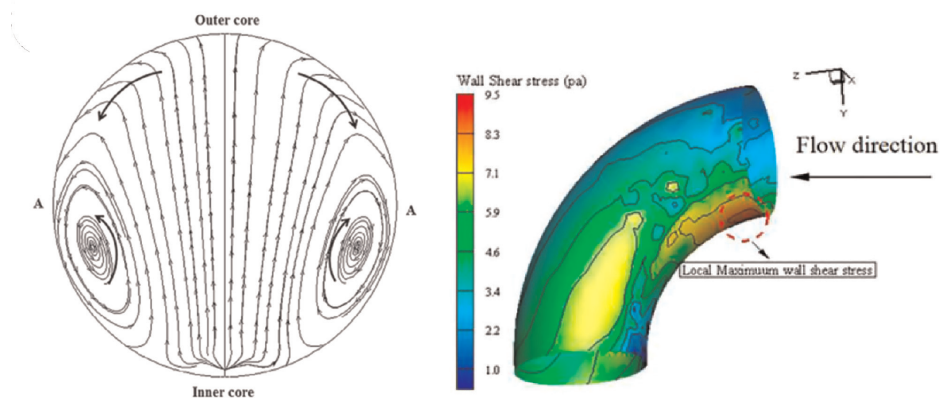
(a) Velocity (Dean vortices) streamlines for 90° elbow [1].

(b) Shear stress along inner wall [2].

Figure 1.
Vortex structure and shear stress distributions along the intrados of typical pipe elbows (from Refs. [2, 15]).

other published research. This study was further developed by Abuhatira et al. [4] who investigated the 90° elbow with normalized radius of curvature of $R_c/D = 2$. Their goal was to determine an optimum turbulence model by selecting a 'balanced' value for Y^+ in order to compromise between computational time on the one hand versus accuracy of results compared to experiment on the other. Abuhatira et al performed a comparative assessment looking at four types of RANS models: k-ε, SST k-Ω, Reynolds Stress Model (RSM) and Spalart-Allmaras to determine which most closely predicted the experimental results published by Sudo et al. [1]. They found RSM is able to predict the steady mean flow spatial structure accurately, but these simulations did not rule out (at least in numerical simulation terms) whether flow unsteadiness plays any role in pipe vortex development. The latter was fully addressed in ref. [16] using Unsteady-RANS simulations and time-stationary nature of vortex flow in the Sudo et al. experiments is discussed at length in this paper.

Notwithstanding the above discussion into the physics of pipe flow, two pertinent issues remain unclear. These are: how the change in working fluid and/or pipe elbow angle has on the spatial development of the vortex. The second is (presumably) the more important of the two. In this paper we, therefore, address both issues. We compare contours of the wall shear stress (WSS) and turbulence kinetic energy (TKE) at bend angles ranging from $(0° - 90°)$ for three types of working fluids commonly used in industrial pipeline flows. That is, air, methane and carbon dioxide. The vortex flow structure obtained in the experiments and simulations (discussed in Wang et al. [12], Abuhatira et al. [4] and more recently in the U-RANS simulations of Church-Forbes et al. [16]) confirm that the maximum shear stress is at the location pipe elbow where the flow turns and vorticity magnitude is greatest. Hence, we focus on the structure of Dean vortices for three fluid types and all bend angles at the elbow location within the pipeline. The simulations were conducted using the Ansys Fluent workbench for pipe flows of fixed geometry that is the same as the airflow experiments conducted in a 90° pipe bend by [1]. The Sudo et al. experiments were validated using steady RANS by [4] and more recently via U-RANS simulation in Church-Forbes et al. [16]. Since the latter indicate that Dean vortices are largely time-invariant, we assess the impact of pipe bend angle using a steady RANS calculation. For the non-air gas flows cases we keep the mass flow rate $(\dot{m})$ fixed and determine the inlet velocity and Reynolds number using the thermodynamic properties of methane and carbon dioxide at standard room temperature. The pipe inlet velocity, elbow angle, Reynolds and Dean numbers are summarized in (**Table 1**).

Our results show that the wall shear stress increases with elbow angle with Dean vortex being fully developed at the intrados location for the 90° bend angle. Although the spatial structure of the Dean vortex is not unaltered by the use of alternative pipe working gas (at fixed bend angle, θ), the magnitude of shear stress and turbulence kinetic energy is effected wing to the difference in inlet flow velocities for pipe flow simulations at fixed mass flow rate. The main physical change that occurs when both working fluid and bend angle are altered in the flow simulations is the intensification of vortex energy (i.e. turbulence kinetic energy associated with the streamwise flow) is greater in magnitude as $\theta \to 90°$ when the inflow velocity is greater. We discuss these results in comparison to the baseline case of airflow at the 90° bend angle corresponding to a Dean vortex with maximum vorticity magnitude. In §.3 we describe the pre-processing required for the Fluent CFD methodology. In Section 4, we present the main results of the paper with a full description of the fluid mechanics of the Dean vortex in terms of streamwise mean velocity distribution, wall shear stress

Case	Gas	Elbow angle	Inlet velocity (ms^{-1})	Re. No.	Dean No.
1	Air	90°	8.427	60,000	30,000
2	Air	60°	8.427	60,000	30,000
3	Air	45°	8.427	60,000	30,000
4	Air	30°	8.427	60,000	30,000
5	Air	0°	8.427	60,000	30,000
6	Methane	90°	15.421	99,385.50	49692.75
7	Methane	60°	15.421	99,385.50	49692.75
8	Methane	45°	15.421	99,385.50	49692.75
9	Methane	30°	15.421	99,385.50	49692.75
10	Methane	0°	15.421	99,385.50	49692.75
11	Carbon Dioxide	90°	5.762	78,199.68	39099.84
12	Carbon Dioxide	60°	5.762	78,199.68	39099.84
13	Carbon Dioxide	45°	5.762	78,199.68	39099.84
14	Carbon Dioxide	30°	5.762	78,199.68	39099.84
15	Carbon Dioxide	0°	5.762	78,199.68	39099.84

Table 1.
Test cases investigated.

distributions and turbulence kinetic energy as a function of pipe bend angle and inflow working fluid.

3. CFD methodology of Church-Forbes et al.

We follow the CFD methodology of Church-Forbes et al. [16], which we remind the reader is based on the Abuhatira et al. [4] mesh that itself is a reproduction of the Sudo et al. [1] experiment. With this in mind, consider a fully developed turbulent flow at inlet to the pipe (**Figure 2**). The flow turns through a bend of angle θ with radius of curvature, $R_c/D = 2$. Adopting a cylindrical coordinate system given (x, r, ϕ), to represent the flow in the pipe, where the velocity $\boldsymbol{v}(\boldsymbol{x}, t) = (u, v_r, v_\phi)(\boldsymbol{x}, t)$ enters at inflow with a streamwise component, $\boldsymbol{v}(\boldsymbol{x}, t) = \boldsymbol{e}_1 U_0$ where $u(x, t) = U_0$ is the constant mean flow.

The pipe geometry is created using the SolidWorks 3D modeling software mainly due to its ease of use but also because of its ability to export the CAD model as an IGES file into Fluent's meshing software. The pipe elbow is modeled according to the dimensions set in the Abuhatira et al. [4] paper, in which a round pipe with a 90° elbow bend downwards has dimensions upstream of the elbow set as $10D$ and downstream at, $20D$. The normalized radius of curvature, $R_c/D = 2$ is kept constant at throughout to keep the geometry in line with Sudo et al. [1], Abuhatira et al. [4], and Kim et al. [3] papers. Abuhatira et al. measure the pipe diameter of the Sudo et al. [1] experimental setup as 0.104 m. But note that the experimental setup in [1] included a longer upstream section but this was reduced by Abuhatira et al. due to the flow being fully developed within a shorter, $10D$ length from inlet [4, 16], which we follow in our
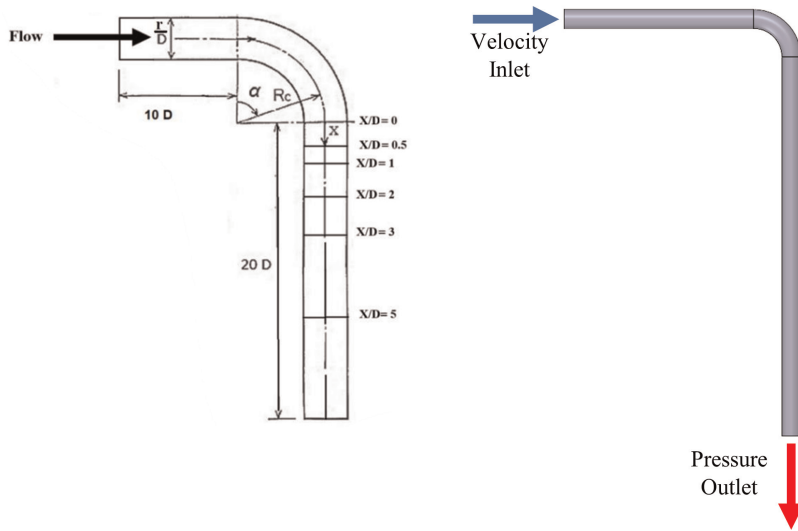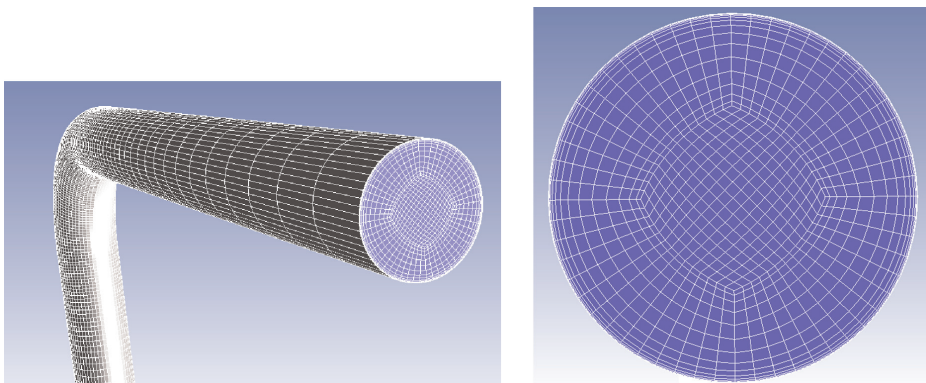
Figure 2.
90-degree pipe elbow schematic reprinted from Abuhatira et al. [4] paper and SolidWorks generated 3D pipe elbow geometry outlining direction of flow.

work here. The mesh for varying elbow angles (**Table 1**) can be easily created by adjusting the elbow curvature (denoted by α in the Abuhatira et al paper reproduced in **Figure 2** and measured from the outlet section to the straight line extending parallel to the inlet) directly in SolidWorks–note that this is a more efficient method than creating new geometries each time. The SolidWorks CAD model can be seen alongside the schematic of the pipe elbow [4] in **Figures 2** and **3**.

The meshing of the pipe elbow is carried out using the inbuilt Ansys meshing tool (after inputting the Solid Works CAD rendering). The Y^+ value at the wall is required to remain less than 3.0 throughout the pipe wall to ensure that the viscous sublayer is adequately resolved following the turbulence model optimization guidelines of

(a) Medium mesh of pipe elbow showing inflation layers on inlet to pipe and structured mesh across body of pipe

(b) Zoomed section at inlet showing inflation layers

Figure 3.
Meshing of pipe elbow using Ansys Fluent built-in meshing.

Abuhatira et al. (see recommendations in [4]). Although, the Y+ value varies along the wall, as noted in the above papers, ensuring the maximum value stays below a certain size is a good way to control it. Using the meshing rules in an inflation layer is added to the inlet and outlet faces, with first cell size set at 1.000756×10^{-4}m designed to remain consistent with the upper bound for Y^+. The remaining geometry can now be meshed with a standard cylindrical mesh having elements of length 1.0×10^{-2}m. The total mesh volume is then 159, 422 elements, which from the grid resolution study in ref. [16] was deemed good enough to achieve converged outlet velocity. The mesh for different bend angles follow similarly but with the finer mesh using a lower value of element size near the elbow section. The skewness of the mesh is kept below 0.95 in all cases (see methodology for the 90° bend angle reported by ref. [16]).

The turbulence model and material settings are fixed in the setup tab in Fluent at the Abuhatira et al. values (i.e., the standard k-ϵ with enhanced wall function with model constants were left at default; and aluminum being chosen for as pipe solid material consistent with the Sudo et al. experiment). The boundary conditions were setup with the gauge pressure of 0 MPa at outlet and the inlet velocity set at 8.427ms^{-1} corresponded to a Reynolds number of Re 60,000 used in [1]. Flow initialization can then begin at the uniform flow velocity at inlet consistent with the experimental setup in Sudo et al. [1]. Spatial discretization was set to second order to ensure the accuracy for a maximum of 2000 iterations which is found to be adequate to achieve residuals of $O(10^{-10})$. Further details regarding the optimum choice on turbulence model, grid convergence study, post-processing of flow data and a detailed comparison with the Sudo et al. experiment and Abuhatira et al.'s study can be found in Church-Forbes et al. [16]. The test cases used in this paper are summarized in **Table 1** and the mesh is depicted in **Figure 3**.

4. Effect of pipe elbow bend angle and working fluid on vortex energy spatial distribution

We consider the two basic parameters of the wall shear stress, $\tau_w = \mu(\partial U(\boldsymbol{x}))/\partial r)|_{r=0}$, and the turbulence kinetic energy (k), to assess the strength of the vortex at the pipe elbow. These results are given in **Figures 4** and **5**. We also compare the velocity streamlines pattern in **Figure 6** to discern the localization of vortex lobes within the pipe as θ increases. All contours are taken at the inlet or exit to the elbow (see caption in **Figures 5–6**). For example **Figure 6a,b** and **c** displays how the velocity streamlines at the elbow exit vary between elbow angles for each fluid type. The legend shown in the bottom of each figures is used to show where the highest velocities occurs in each elbow exit, and this is observed to occur near the middle of the pipe for each elbow configuration. At 90° (on far left of each row) there is a high degree of separation in the flow and swirling occurs in the form of eddies in the contours at the inside pipe wall. This data correlates well with the velocity profiles found in literature (see **Figure 7** and further discussion in §. 5). At 60°, separation starts to decrease to a lesser degree and moves towards the walls perpendicular to the inside wall. The 30° contours appears to be the most structured of the four elbow angles, with the eddies occurring only towards the wall perpendicular to the inside and outside walls. The limit of this trend is consistent with the flow features of Wang's results (reproduced in **Figure 7**) for the 0° bend angle (straight pipe) test case.
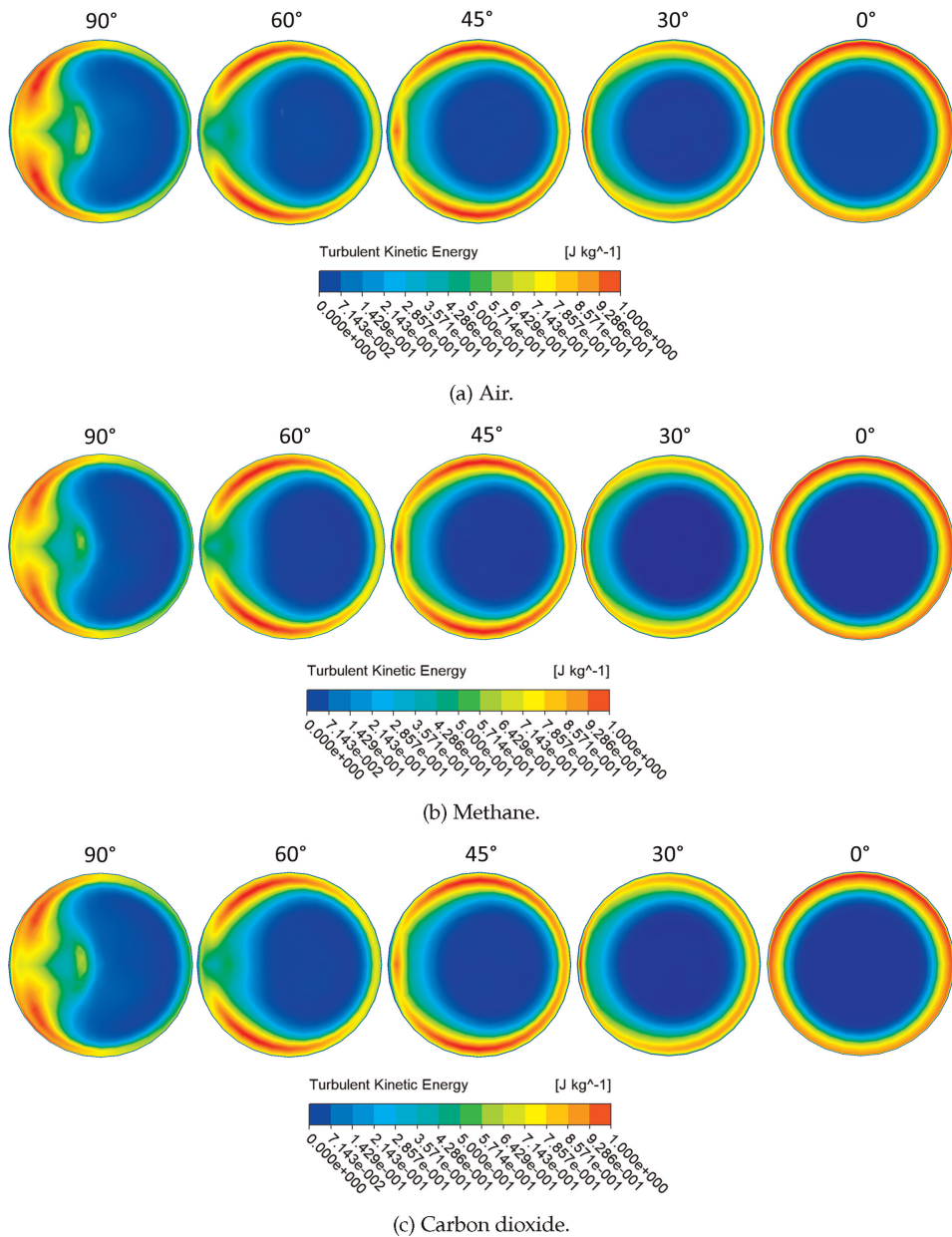
(a) Air.

(b) Methane.

(c) Carbon dioxide.

Figure 4.
Contours of turbulent kinetic energy $k(x)$ at elbow inlet for $(90°, 60°, 45°, 30°)$ pipe elbow bend angles under different working fluid.

4.1 Variation of $\max \tau_w(x)$ and $\max k(x)$ with working fluid at fixed θ

Figure 8 shows the change in maximum value of the wall shear stress at the different elbow angles in **Table 1** (ranging from $30° - 90°$). As expected, τ_w increases more or less proportionally with θ for each working fluid. Taking air between bend angles between $30° - 45°$ for example, τ_w increases by 2.85% from 0.424 Pa to
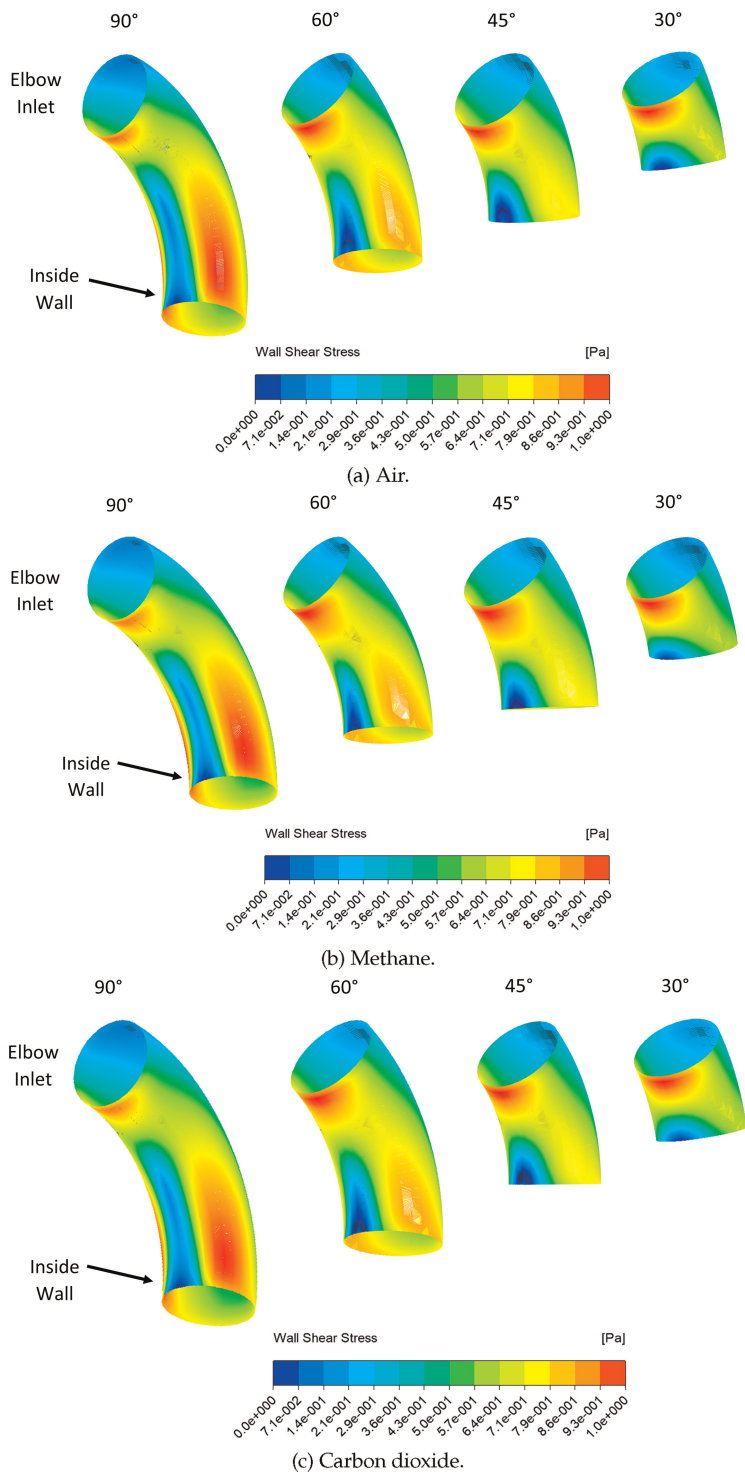
Figure 5.
Wall shear stress (τ_w) distribution along the wall of pipe at (90°, 60°, 45°, 30°) elbow bend angles under different working fluids.
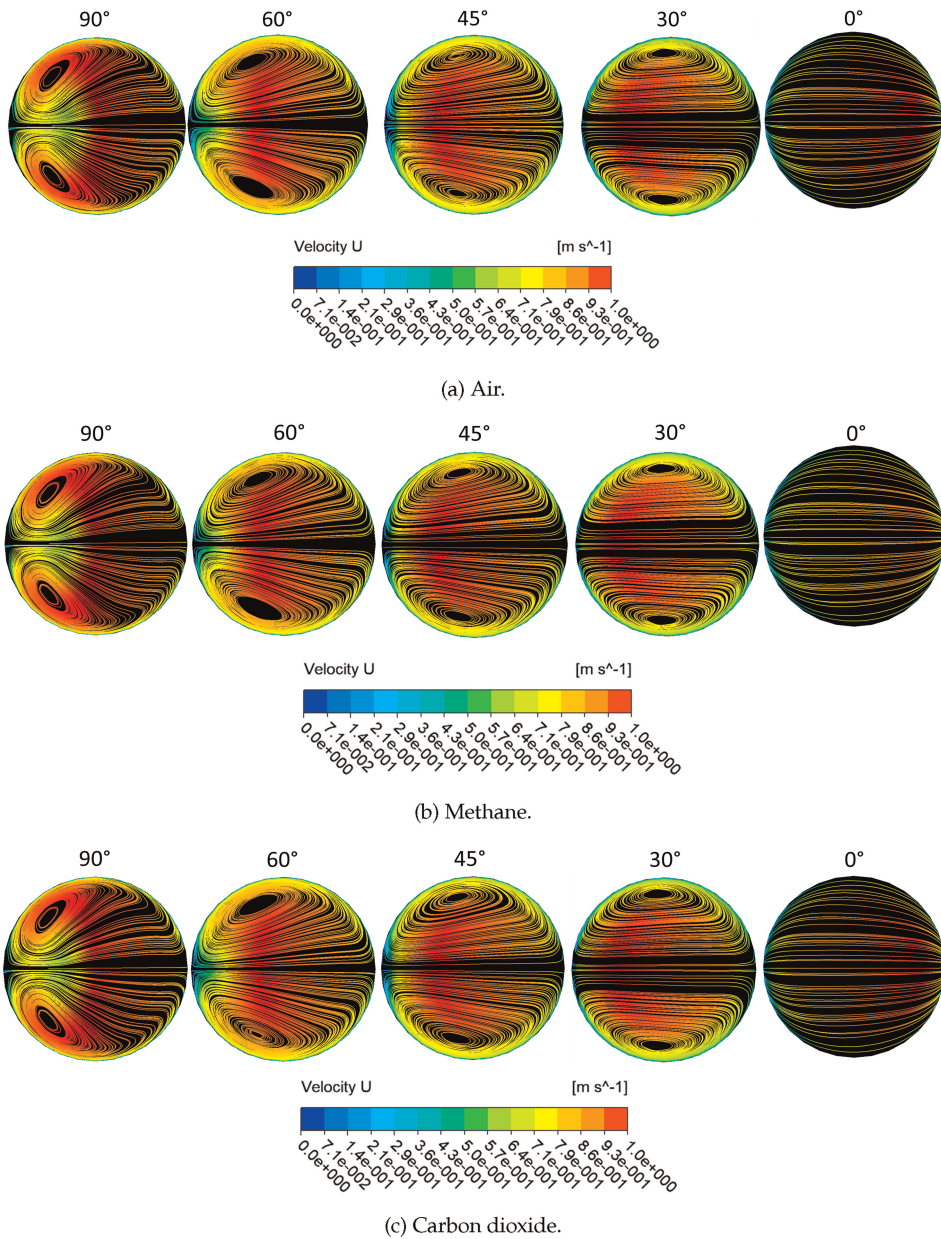
(a) Air.

(b) Methane.

(c) Carbon dioxide.

Figure 6.
Velocity streamlines $\overline{u}(\boldsymbol{x};\theta)$ at elbow exit for $(90°, 60°, 45°, 30°)$ pipe elbow bend angles under different working fluid.

0.436 Pa (3 d.p.). Interestingly, between elbow angles of 45° and 60°, there is little to no change in τ_w, with numerical variation of 0.436 Pa to 0.439 Pa, which correspond to about 0.65% difference between the two cases. Not surprisingly, the largest difference is between the angles of 60° and 90° which results in a 6.2% increase in τ_w. The individual wall shear stress surface contours are displayed in **Figure 5a–c**.

Figure 7.
Velocity streamlines (Wang et al. [12]) at elbow locations of 90°, 60°, 45° and 30° with 0° at the elbow inlet.
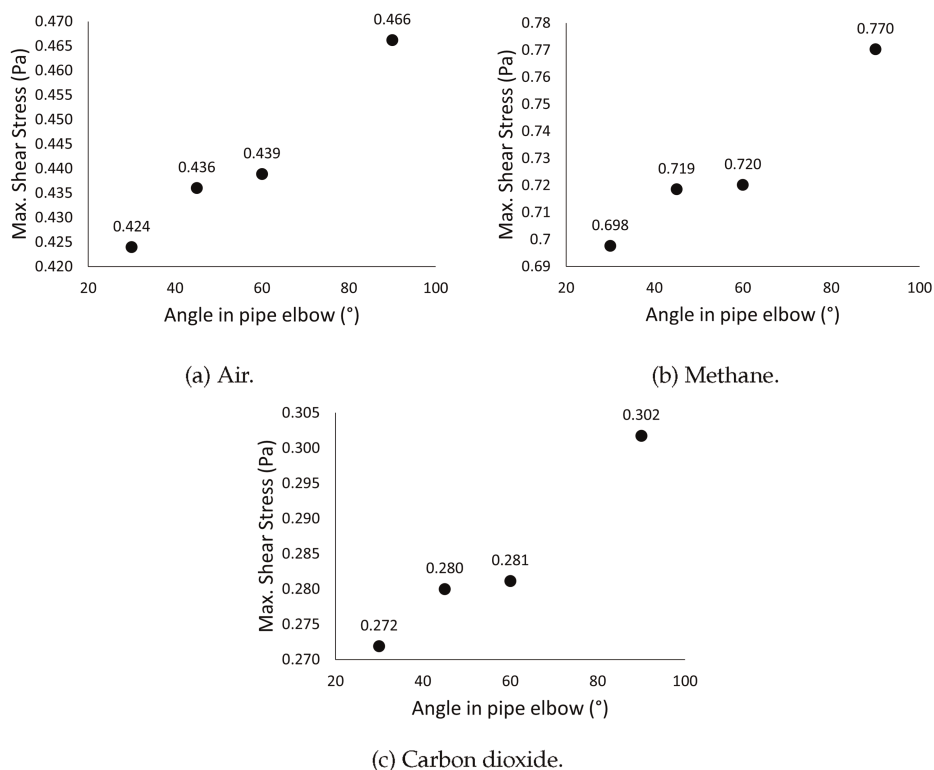

(a) Air.

(b) Methane.

(c) Carbon dioxide.

Figure 8.
Wall shear stress (τ_w) at the elbow exit plane in **Figure 5** *as a function of bend angle θ.*

The 90° (**Figure 5a** for air) elbow exhibits the highest shear stress at inlet to the bend. The high τ_w at the perpendicular walls in the 90° elbow is consistent with the high velocity values apparent at these locations in the pipe (see **Figure 6a** for air and cf. **Figure 6b** and **c**).

The main differences in τ_w distribution over the pipe surface when using methane/carbon dioxide as working fluid is the higher/lower values for magnitude of shear stress. This is direct consequence of the fixed inlet mass flow rate through the pipe and increased/decreased inlet velocity (**Table 1**). While the spatial distributions for wall shear stress in **Figure 5** is virtually the same for all working fluids (e.g. compare **Figure 4a-b** and similarly compare 7a to 7b). But, nonetheless, the higher/lower
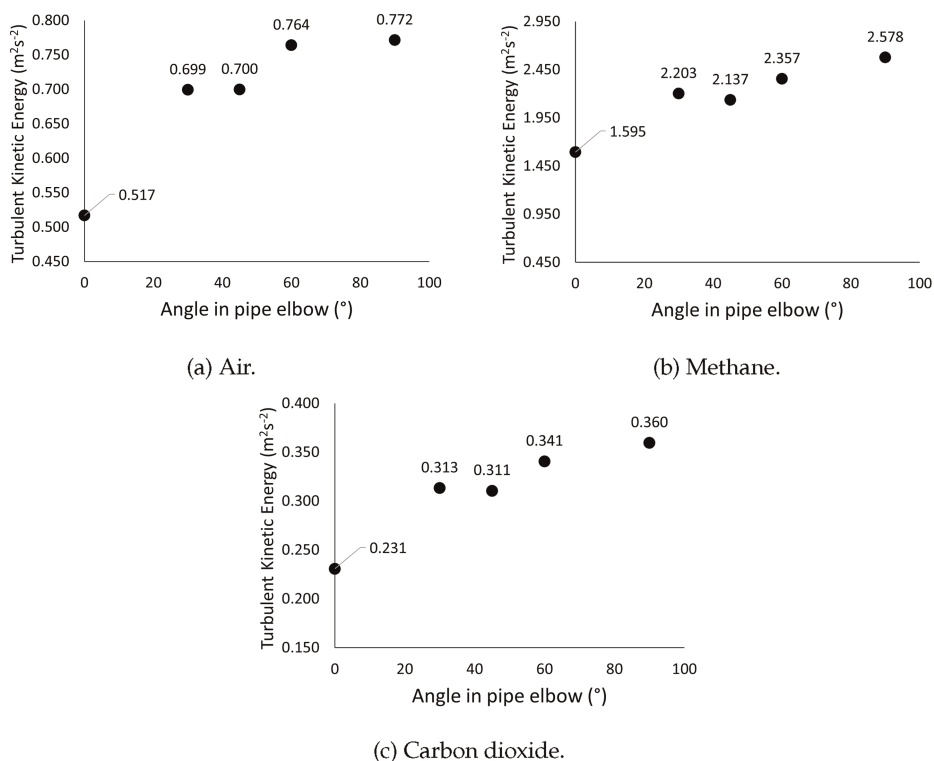
(a) Air.

(b) Methane.

(c) Carbon dioxide.

Figure 9.
*max $k(\boldsymbol{x})$ at the elbow exit plane in **Figure 4** as a function of bend angle θ.*

inflow velocity for methane/carbon dioxide compared to air, will result is higher/ lower numerical values for the maximum wall shear stress (WSS) at the intrados location. This can be easily observed in the distribution of max $\tau_{\mathrm{w}}(\boldsymbol{x})$ values with θ in **Figure 8a–c**. At any fixed value of bend angle θ, while almost doubling when air and methane (**Figure 8a** vs. **b**), will almost halve in value when carbon dioxide is used (**Figure 8c**). Note, that for all three working fluids max $\tau_{\mathrm{w}}(\boldsymbol{x}) < 1$.

The turbulence kinetic energy defined in cylindrical polar velocity components is given by $2k(\boldsymbol{x}) = \left(\overline{u'^2 + v_r'^2 + v_\phi'^2} \right)(\boldsymbol{x})$ where the velocity perturbation $\boldsymbol{v}'(\boldsymbol{x}, t) = \{u', v_r', v_\phi'\}(\boldsymbol{x}, t) = \boldsymbol{v}(\boldsymbol{x}, t) - \overline{\boldsymbol{v}}(\boldsymbol{x})$ is defined about the time averaged mean flow:

$$\overline{\boldsymbol{v}}(\boldsymbol{x}) = \lim_{T \to \infty} \frac{1}{2T} \int_{-T}^{T} \boldsymbol{v}(\boldsymbol{x}, t) \, dt \tag{1}$$

where $\overline{\boldsymbol{v}}(\boldsymbol{x}) = \left(\overline{u}, \overline{v}_r, \overline{v}_\phi \right)(\boldsymbol{x})$ is given directly by the Fluent CFD calculation in which the average flow quantities are determined over the simulation time, T. In **Figure 4** we show the $k(\boldsymbol{x})$ distribution for all working fluids across bend angles, $\theta = (0° - 90°)$. As expected, the maximum in the TKE distribution at elbow exit is proportional to the the inflow pipe velocity. The methane results in **Figure 9b** are higher than both air and carbon dioxide in **Figure 9a** and **c**. The distribution of max $k(\boldsymbol{x})$ values at the

elbow exit plane in **Figure 9a** vs. **b** and **c** shows methane as the working fluid will result in an almost three-fold increase in turbulence kinetic energy compared to air. Carbon dioxide, on the other hand, results in almost a halving of max $k(x)$ values compared to air (**Figure 9c** vs. **a**).

4.2 Variation of max $\tau_w(x)$ and max $k(x)$ with θ at fixed working fluid

The mean flow simulation results in **Figures 4** and **5** show that maximum vortex intensification occurs at at the 90° bend angle. For example, **Figure 8** shows that for $\theta \in [30°, 90°]$, max $\tau_w(x)$ increases from 0.272 Pa to 0.280 Pa at 45° (3% increase) for air. Methane as the working fluid results in an increase of max $\tau_w(x)$ of 0.4% to 0.281 Pa. Again, the largest increase in wall shear stress at the elbow is observed between 60° and 90° with a 7.33% change to a maximum value of 0.302 Pa. While the magnitudes of $\tau_w(x)$ are smaller for carbon dioxide compared to air and methane, the changes in max $\tau_w(x)$ as θ increases is similar to the trends above. For example, the largest increase in wall shear stress at the elbow is observed at 90° for cabon dioxide under a 7.33% change to a maximum value of 0.302 Pa (**Figure 8c**).

The change in max $k(x)$ with θ is similar for all working fluids and peaks at $\theta = 90°$. For example, comparing numerical values in **Figure 9a**, the RANS simulation shows that flow turning through a 90° bend will experience a 49.25% increase in max $k(x)$ compared to $\theta = 0°$. Using methane (**Figure 9b**) or carbon dioxide (**Figure 9c**) increases/decreases this change compared to $\theta = 0°$ to 61.65%/55.80% respectively. Note that the overall trend of $k(x)$ increasing with θ is not the case for every elbow angle and gas combination; for example, methane and carbon dioxide experience a smaller decrease between 30° and 45° compared to the percentage change in $k(x)$ between 60° to 90°. The reason for this apparent 'intermediate leveling' of $k(x)$ with bend angle (see **Figures 8–10** and **Table 2**) is unexplained within our findings and would be an interesting avenue for mathematical modeling.
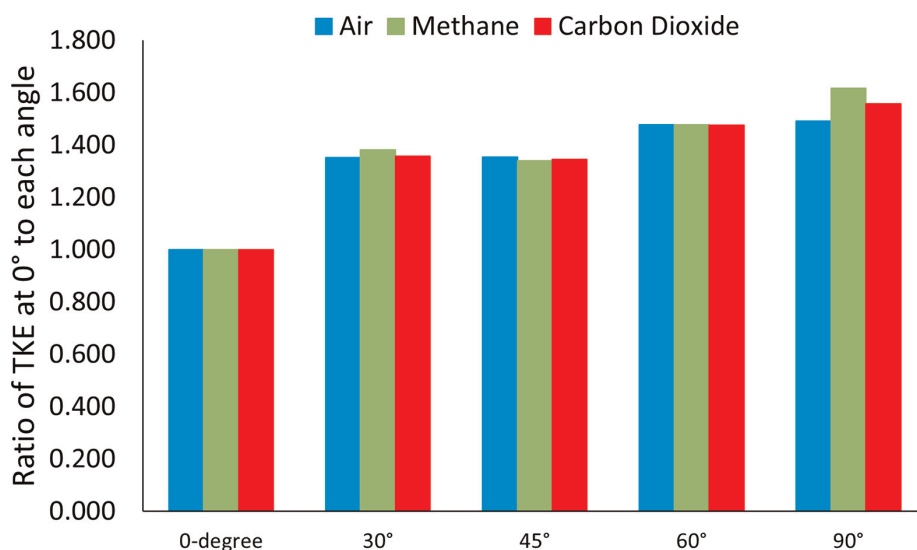

Figure 10.
max $k(\theta) /$ max $k(\theta = 0°)$ *with working fluid.*

Gas	Elbow Angle	TKE (m^2s^{-2})
Air	90°	0.772
Air	60°	0.764
Air	45°	0.700
Air	30°	0.699
Air	0°	0.517
Methane	90°	2.578
Methane	60°	2.357
Methane	45°	2.137
Methane	30°	2.203
Methane	0°	1.595
Carbon Dioxide	90°	0.360
Carbon Dioxide	60°	0.341
Carbon Dioxide	45°	0.311
Carbon Dioxide	30°	0.313
Carbon Dioxide	0°	0.231

Table 2.
max $k(x)$ at varying bend angle, θ.

5. Discussion: Consistency of results

Flow simulations reported in this paper reveal that at the intrados location near the elbow inlet there will be a higher shear stress (**Figure 5**). $\tau_w(x)$ reduces at elbow exit on the intrados location for each bend angle, θ, and for any working fluid. The 90° elbow bend angle exhibits a high wall shear stress at the walls perpendicular to the inside and outside walls. Intense $\tau_w(x)$ is also visible on the 60° elbow but to a lesser degree and is not found on the 45° and 30° elbows (cf. contours at each θ in **Figure 5a, b** or **c**). **Figure 4a-c** display $k(x)$ contours at elbow inlet for all gases as θ reduces from
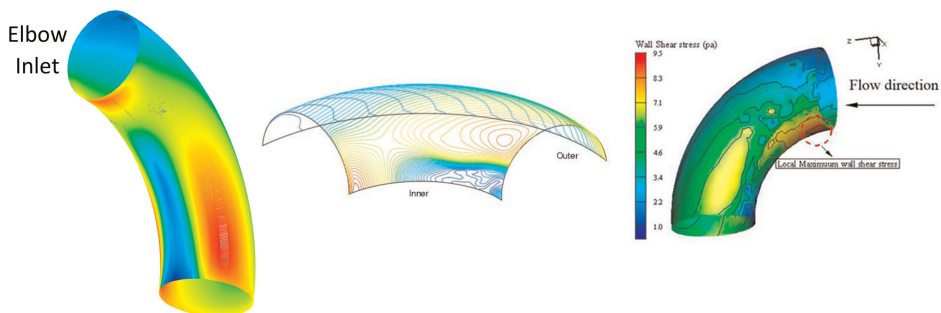

Figure 11.
Comparison between wall shear stress contours our simulations for air at 90° (left) and Homicz et al. (middle) and Liu et al. [15] (right).

90° to 30° compared to 0° (straight pipe). $k(\boldsymbol{x})$ is a maximum at the inner wall (red color in contours) for the 90° bend angle. Indeed, the contour at 0-degrees was found to correlate well with results in [18] which also showed the minimum TKE occur at the middle of the pipe.

Homicz et al. investigated pipe elbows in the nuclear power industry using the Fluent software. The $\tau_w(\boldsymbol{x})$ contours at 90° from our RANS simulations match the Homicz et al. results (see **Figure 11**) with the max $\tau_w(\boldsymbol{x})$ occurring at the intrados of the elbow inlet and outer pipe walls. The wall shear stress contours at 90° were also compared with Liu et al. [15] who investigated max $\tau_w(\boldsymbol{x})$ for a corrosion effect study of water and oil mixture in a steel pipeline.

Work published by Dutta et al. [2] also found Dean Vortices at the 90° location consistent with our results. Wang et al. [12] published velocity streamline data at 0° (elbow inlet) and 90° (elbow exit) and also observed such vortices (See **Figure 7**). In comparing velocity streamlines for all working fluids (**Figure 6a-c**) with Wang et al. [12] (**Figure 7**), we find a reasonable degree of spatial similarity between both datasets (theirs and ours) indicating further consistency of present results.

6. Conclusions

In this paper, we conducted a computational fluid dynamics (CFD) study using steady Reynolds-averaged Navier-Stokes (RANS) simulations of flow through an industrial flow pipeline carrying a different working fluid and and elbow angle (θ) measured from the horizontal inflow section. Understanding the magnitude of wall shear stress and maximum turbulence kinetic energy are important parameters in monitoring overall pipe longevity (high shear stress is linked to higher levels of corrosion; see ref. [15]). Our results show that commercial RANS CFD simulations are capable of determining the effect of the elbow angle on the wall shear stress and turbulence kinetic energy effectively. We investigated three working gases (air, methane & carbon dioxide) at fixed inflow mass flow rate for pipe geometry based on the Sudo et al. [1] experiment (also reported in Abuhatira et al. [4]). The elbow angles ranging from $\theta = [0°, 30°, 45°, 60°, 90°]$. Our results show that while working gas does not change the spatial structure of the turbulence kinetic energy and wall shear stress distribution compared to baseline calculation for air flow (as used in refs. [1, 4]), their magnitudes are affected because the inflow velocity is increased/decreased depending on the working gas density relative to air. The velocity stream-lines visible in **Figure 6a-c** can be observed to show the same trend for all three gases. The 90° elbow exhibits the highest degree of recirculation in the flow shown near the inner wall (Dean vortices). These vortices are caused by the centrifugal force and viscous forces being at their maximum at this location within the flow [12] and are weakened as the elbow angle approaches the $\theta = 0°$ straight pipe configuration. Reducing the elbow angle (θ), reduces the wall shear stress. Reducing the elbow angle from 90° to 60° was found to result in the greatest percentage reduction in wall shear stress value (see **Figure 8**) for all working fluids. This could be used for industrial applications when designing pipeline systems with increase system longevity in mind.

The methodology and results of the present paper can be used for industrial flow problems (e.g. as in the Sudo et al. [1] and Abuhatira et al. studies) or medical flow problems e.g., determining surface shear stress on skin grafts [16] that are required to be within certain tolerances for maximum longevity.

Author details

Keagan Church-Forbes[1], Mohammad Zamir A. Koshuriyan[2*] and
Ahmed A. Abuhatira[3]

1 Department of Mechanical and Aerospace Engineering, University of Strathclyde, Glasgow, UK

2 Department of Mathematics, University of York, Heslington York, UK

3 Nuclear, HE Engineering and Science, Lakes College West Cumbria, Workington, UK

*Address all correspondence to: zamir.koshuriyan@york.ac.uk

IntechOpen

References

[1] Sudo K, Sumida M, Hibara H. Experimental investigation on turbulent flow in a circular-sectioned 90-degree bend. Experiments in Fluids. 1998;**25**(1):42-49

[2] Dutta P, Saha S, Nandi N, Pal N. Numerical study on flow separation in 90° pipe bend under high Reynolds number by k- modelling. Engineering Science and Technology, an International Journal. 2016:904-910

[3] Kim J, Yadav M, Kim S. Characteristics of secondary flow induced by 90-degree elbow in turbulent pipe flow. Engineering Applications of Computational Fluid Mechanics. 2014;**8**(2):229-239

[4] Abuhatira AA, Salim SM, Vorstius JB. Numerical simulation of turbulent pipe flow with 90-degree elbow using wall Y+ approach. In: Proceedings of the ASME 2021 International Mechanical Engineering Congress and Exposition IMECE2021. IMECE2021 November 1-5, 2021, Virtual, Online

[5] Röhrig R, Jakirlić S, Tropea C. Comparative computational study of turbulent flow in a 90° pipe elbow Author links open overlay panel. International Journal of Heat and Fluid Flow. 2015;**55**:120-131

[6] Wang S, Ren C, Sun Y, Yang X, Tu J. A study on the instantaneous turbulent flow field in a 90-degree elbow pipe with circular section. Science and Technology of Nuclear Installations. 2016;**2016**:e5265748

[7] Dutta P, Nandi N. Effect of Reynolds number and curvature ratio on single phase turbulent flow in pipe bends. Mechanics and Mechanical Engineering. 2015;**19**:5-16

[8] Hufnagel L, Canton J, Örlü R, Marin O, Merzari E, Schlatter P. The three-dimensional structure of swirl-switching in bent pipe flow. Journal of Fluid Mechanics. 2018;**835**:86-101

[9] Korei Z, Benissaad S. Turbulent forced convection and entropy analysis of a nanofluid through a 3D 90° elbow using a two-phase approach. Heat Transfer. 2021;**50**(8):8173-8203

[10] Mazumder Q, Nallamothu VT, Mazumder F. Comparison of characteristic particle velocities in solid-liquid multiphase flow in elbow. International Journal of Thermofluids. 2020;**5–6**:100032

[11] Ganesh N, Jain P, Choudhury A, Dutta P, Kalita K, Barsocchi P. Random forest regression-based machine learning model for accurate estimation of fluid flow in curved pipes. PRO. 2021;**9**(1111):2095

[12] Wang Y, Dong Q, Wang P. Numerical investigation on fluid flow in a 90-degree curved pipe with large curvature ratio. Mathematical Problems in Engineering. 2015;**2015**:1-12

[13] Zhang P, Gros Y, Roberts R, Benard A. Modeling of Turbulent Flow with Particle Deposition in Curved Pipes. Tampa, FL USA: 7th International Conference on Multiphase Flow ICMF; 2010; May 30-June 4, 2010

[14] Bernad SI, Totorean A, Bosioc A, Stanciu R, Bernad ES. Numerical investigation of Dean vortices in a curved pipe. AIP Conf. Proc. 2013;**1558**:172-175

[15] Liu X, Gong C, Zhang L, Jin H, Wang C. Numerical study of the hydrodynamic

parameters influencing internal corrosion in pipelines for different elbow flow configurations. Engineering Applications of Computational Fluid Mechanics. 2020;**14**(1):122-135

[16] Church-Forbes K, Koshuriyan MZA, Abuhatira AA. CFD investigation of unsteady fluid effects through industrial flow pipelines and pipe elbows, Submitted to Proc. IMechE Part C. Journal of Mechanical Engineering Science. 2024